Threshold of vapor pressure deficit constraint on light use efficiency varied with soil water content

Dexin Gao[1]; Shuai Wang[1]; Zidong Li[1]; Fangli Wei[2]; Peng Chen[1]; Shuang Song[1]; Yaping Wang[1]; Lixin Wang[3]; Bojie Fu[1,2]

[1] *State Key Laboratory of Earth Surface Processes and Resource Ecology, Faculty of Geographical Science, Beijing Normal University, Beijing*, 100875, China

[2] *State Key Laboratory of Urban and Regional Ecology, Research Center for Eco-Environmental Sciences, Chinese Academy of Sciences, Beijing*, 100085, China

[3] *Department of Earth Sciences, Indiana University–Purdue University Indianapolis (IUPUI), Indianapolis 46202, United States*

Correspondence

Wang Shuai, *Faculty of Geographical Science, Beijing Normal University*, *Beijing*, 100875, China

Email: shuaiwang@bnu.edu.cn

Abstract: Understanding the constraints on light-use efficiency (*LUE*) induced by high evaporative water demand (vapor-pressure deficit; *VPD*) and soil water stress (soil moisture content; *SMC*) is crucial for understanding and simulating vegetation productivity, particularly in the arid and semi-arid regions. However, the relative impacts of *VPD* and *SMC* on *LUE* are unclear, as we lack a mechanistic understanding of impacts and their interactions. In this study, we quantified the relative roles of *VPD* and *SMC* in limiting *LUE* and analyzed the interactions among *VPD*, *SMC*, and *LUE* using data from CO_2 and water flux stations and weather stations along a climatic gradient in the Heihe River Basin, China. We found a threshold of *VPD* constraint on *LUE*; above the threshold, *LUE* decreased at only 3.6% to 23.1% of the rate below the threshold. As *SMC* decreased, however, the *VPD* threshold increased, and the reduction of *LUE* caused by *VPD* decreased significantly, which is more than half of that in moister regions. Therefore, both *VPD* and *SMC* played essential roles in *LUE* limitation caused by water stress. A threshold also existed for heat flux and the correlation between *SMC* and *LUE*; the strength of the correlation first decreased and then increased with increasing *VPD*. Our results clarified

---

This is the author's manuscript of the article published in final edited form as:

Gao, D., Wang, S., Li, Z., Wei, F., Chen, P., Song, S., Wang, Y., Wang, L., & Fu, B. (2022). Threshold of vapour–pressure deficit constraint on light use efficiency varied with soil water content. Ecohydrology, 15(5), e2305. https://doi.org/10.1002/eco.2305

the relative impacts of *VPD* and *SMC* on *LUE*, and can improve simulation and prediction of plant productivity.

Keywords: *VPD*, *SMC*, *LUE*, threshold, carbon simulation uncertainty, dryland

1. Introduction

Atmospheric water demand, which is defined by the vapor-pressure deficit (*VPD*), and soil water supply (soil moisture content; *SMC*) together determine the level of plant water stress, and strongly affects photosynthesis. Light use efficiency (*LUE*), defined as the ratio of productivity and intercepted radiation (Monteith et al., 1977), tightly couples with plant transpiration and stomatal conductance (Novick et al., 2016). Stomatal conductance directly responds to rising *VPD* (Fletcher et al., 2007). High levels of *VPD* decrease stomatal conductance (Grossiord et al., 2020) and lead to reduction of *LUE* (Wu et al., 2013). *SMC* is the direct source of available water for plants to maintain photosynthesis (Trugman et al., 2018) and insufficient *SMC* can decrease photosynthesis (Bartlett et al., 2016). Water stress can decrease the conductance of stem and stoma, resulting in significant decrease in photosynthesis (Mccarter and Price, 2014; Taylor et al., 2016). Overall, both *VPD* and *SMC* strongly affect plants *LUE* and carbon budget (Rigden et al., 2020). *VPD* and *SMC* change significantly over time in response to changes in temperature and precipitation (Stocker et al., 2013). *VPD* will significantly increase with rising temperatures (McDowell and Allen, 2015; Yuan et al., 2019). However, the response of *SMC* to climate change is uncertain, since some regions will experience increased precipitation and others will experience decreased precipitation (Stocker et al., 2013). The different trajectories of *VPD* and *SMC* require a better understanding of *VPD* and *SMC* controls on plant water stress under climate change. Thus, studying the effects of *VPD* and *SMC* on *LUE* is necessary to support simulation and prediction of future plant productivity.

The relative importance of *VPD* and *SMC* in the regulation of photosynthesis remain

unclear, leading to large uncertainty in productivity simulations (Stocker et al., 2019; Yuan et al., 2014). Some studies have found that increasing *VPD* can significantly decrease vegetation productivity by causing declines in carbon uptake and plant growth (Novick et al., 2016, Yuan et al., 2019). However, *SMC* constraint on *LUE* indicated that *SMC* was so important that would cause 40% reduction of *LUE* (Stocker et al., 2018). Effect of *SMC* on photosynthesis would further increase after decoupling *VPD* and *SMC*, whereas constraint of *VPD* decreased (Liu et al., 2020). On the other hand, both *VPD* and *SMC* are essential for simulation of crop yield. Accounting for only *VPD* would lead to overestimate of the yield loss caused by water stress by a factor of two (Rigden et al., 2020).

Both *VPD* and *SMC* play important roles in plant water stress but through different mechanisms: *VPD* affects water demand whereas *SMC* affects water supply (Hsiao et al., 2019). Furthermore, there is inherent correlation between *VPD* and *SMC*, so the two factors interact to determine plant water status, which regulates *LUE* (Novick et al., 2016). Thus, disagreement over their relative importance may result from different perspectives on how *VPD* and *SMC* affect *LUE* and how *VPD* interacts with *SMC*. The relative magnitudes of the impacts of *SMC* and *VPD* on photosynthesis and the associated mechanisms remain unclear (Liu et al., 2020; Seneviratne et al., 2010). It is therefore necessary to study how *VPD* and *SMC* constrain *LUE*, particularly at a regional-scale. Accounting for these constraints in regional scale would decrease the uncertainty caused by other factors, such as difference in N deposition and soil texture in different regions (Lanning et al., 2019).

To provide insights into these factors, we performed a study in the Heihe River Basin in China, where heat and CO_2 fluxes are measured and weather stations have been established along a climate gradient. This paper aims to understand the relative impacts of *VPD* and *SMC* on *LUE*, thereby providing an improved basis for simulating and predicting vegetation productivity. Specifically, we studied the interaction between *VPD*, *SMC* and *LUE* to clarify

(1) the relative constraining effect of *VPD* and *SMC*, and (2) the process of constraining by *VPD* and *SMC*.

2. Methods

2.1. Study area

The Heihe River Basin covers an 821-km length of rivers in an area of 1.429×10^5 km^2, and it is the second largest inland river basin in China (Figure 1). There is strong climatic variation within the basin because of its large size. The mean annual precipitation (*MAP*) ranges from 36 to 444 mm and decreases from south to north. In the upper basin, which covers 1.001×10^4 km^2, *MAP* is more than 350 mm. The middle reaches cover 3.388×10^4 km^2, with *MAP* of 50 to 250 mm. In the lower reaches, however, *MAP* is <50 mm (Wang et al., 2019). In 2015, the HiWATER eco-hydrological observation network was set up in the basin to monitor eco-hydrological processes in the different climate zones (Song, 2019). Eco-hydrological observations include greenhouse gas fluxes and meteorological measurements using the eddy covariance (EC) towers in the Heihe River Basin (Li et al., 2013).

We used field observations from five stations, covering lower to upper reaches. These stations were installed along the climatic gradient at Huyang, Hunhe, Sidaoqiao, Daman, and Arou within the Heihe River Basin (Figure 1 and Table 1). Fluxes data of CO_2, water, and heat were automatically collected by an open-path, infrared gas analyzer (Li-7500, LiCor Inc., USA) and a three-dimensional sonic anemometer (CSAT3, Campbell Inc., USA) (Liu et al., 2011). Five automatic weather stations (AWS) were established to measure air temperatures and humidity (HMP45C,Vaisala), solar radiation (PSP, Eppley and PIP, Eppley), as well as soil temperature (HFP01, Hukeflu), soil heat flux (HFT3, Campbell), and *SMC* (CS616, Campbell Inc., USA) from 4 cm soil layers. Data was recorded by a data logger (CR5000, Campbell Scientific Inc.) at a frequency of 10 Hz for all the stations.

VPD and *SMC* are coupled at monthly and annual scales but tend to be decoupled at a daily scale (Liu et al., 2020; Novick et al., 2016). In this study, half-hour data was used to separate the effects of *VPD* and *SMC*. Half-hour data with high quality of interpolation was selected for analysis including observations in 2013 for Arou, 2015 for Huyang, 2016 for Daman and Sidaoqiao, and 2017 for Hunhe. In our analyses, we only used data collected from July because July is the peak growing season and the variation magnitude of environmental factors are relatively small. In addition, we filtered the data and only included the ones with *PAR* ranging between 500 and 1500 μmol/m^2 to eliminate periods with strong solar radiation, which constrained *LUE* (Cleverly et al., 2020; Novick et al., 2016). The *SMC* constraint on *LUE* was indicated by comparing the effect of *SMC* under different water conditions.

2.2. Flux data quality control, filling, and partitioning

Firstly, 10 Hz data of heat and CO_2 flux were processed by EdiRe software (https://www.campbellsci.com/) to obtain half-hour data. Processing included despiking, coordinate rotation, time lag correction, frequency response correction and Webb–Pearman–Leuning calibration (WPL) (Yu et al., 2006). Secondly, we eliminated the CO_2, water, and heat flux data with low quality. Considering steady state and integral turbulence, the flux data of CO_2, water and energy was classified by different quality level according to quality assessment and control (QA/QC) (Isaac et al., 2017), and we only selected flux data with high quality. Data would be screened if there were precipitation and if the equipment malfunctioned. The data measured at low value of u^* were also excluded. The threshold was 0.1m/s in Arou, 0.2 m/s in Daman, 0.1m/s in Hunhe, and 0.15 m/s in Huyang (Mei et al., 2018). After removing errors and low-quality data, we used the non-liner function methods of Michaelis–Menten (Equation 1) (Falge et al., 2001) and Lloyd-Taylor (Equation 2) (Ahmed et al., 2017) to interpolate missing values (Biederman et al., 2017). The missing values were interpolated by nonlinear fitting, from

which α (initial quantum yield), Pmax(maximum photosynthetic rate), a, and b were derived. We calculated the R^2 of the fitting to assess the quality of interpolation (Falge et al., 2001). R^2 ranged from 0.58 to 0.76 (Table S1). Thus, the interpolation quality was adequate for further analysis.

$$NEE = -\frac{\alpha \times PAR \times P_{max}}{\alpha \times PAR + P_{max}} \quad (1)$$

where *NEE*, α, *PAR*, P_{max} represent net ecosystem exchange, initial quantum yield, photosynthetically active radiation, and the maximum photosynthetic rate, respectively;

$$Reco = a \times exp^{bTs} \quad (2)$$

where *a* and *b* are constants, and *Reco* and *Ts* represent ecosystem respiration and the soil temperature at a depth 5 cm, respectively. We then calculated *GPP* following Fei et al., (2019) :

$$GPP = Reco - NEE \quad (3)$$

There are different definitions of *LUE* (either the ratio of GPP to absorption of photosynthetically active radiation (APAR) or the ratio of GPP to photosynthetically active radiation (PAR)). In this study, ecological *LUE* was used to represent ecosystem *LUE,* which was defined as (Fei et al., 2019):

$$LUE = \frac{GPP}{PAR} \quad (4)$$

VPD was calculated with the following equation (Venturinip et al., 2011):

$$VPD = 0.61078 \times e^{\frac{117.27 \times Ta}{Ta+237.3}} \times (1 - RH) \quad (5)$$

where *Ta* and *RH* represents air temperature and relative humidity, respectively.

2.3. Analysis methods

We analyzed the effect of *SMC* on *LUE* with different soil moisture conditions in four sites as well as one site with significantly variable soil moisture dynamics. We used two methods aiming to strengthen the robustness of our analyses of the impact of *VPD* and *SMC* on *LUE*.

We firstly divided *VPD* data of each site by method of data box (Liu et al., 2020). The *VPD* data was divided into 10 to 15 bins according to the range of *VPD* in different sites. *SMC* of four sites ranged from 30 to 40% at Daman, 20 to 30% at Sidaoqiao, 10 to 20% at Hunhe, and 0 to 10% at Huyang. We used the natural range of *SMC* at each of the four sites and used the four sites together to evaluate the effect of *SMC* constraint on *LUE* under different soil moisture conditions. Arou was a relatively moist site with *SMC* ranging from 10-50%. As such, we selected Arou as a single site to analyze the *SMC* constraint on *LUE* under different soil moisture conditions. The data of *SMC* in Arou was similarly divided into bins of 40-50%, 30-40%, 20-30%, 10-20%.

The piecewise linear regression was used to analyze the relationships between *VPD* and *LUE*. Piecewise linear regression firstly examined whether a break point (threshold) existed in the regression line. Then a linear regression was fitted below and above the threshold. We further examined how the effect of *SMC* on *LUE* varied under different *SMC*. The Pearson's *r* between *LUE* and *SMC* was also calculated. We analyzed the changes of Pearson's *r* with increasing *VPD* to evaluate the interaction of *VPD*, *SMC*, and *LUE*.

We identified the maximum *LUE* value when *VPD* is near zero without *VPD* constraint. We also identified the *LUE* value when *VPD* was near the threshold, exceeding which the *LUE* would not significantly decrease. This *LUE* value was considered the minimum *LUE* value constrained by *VPD*. The difference of maximum and minimum *LUE* constrained by *VPD* was considered the reduction of *LUE*(f*LUE*) constrained by *VPD.* Therefore, we consider the remaining *LUE* (r*LUE*) was not significantly affected by *VPD*. All statistical analyses were performed in Python (https://www.python.org/), and graphs were made using Origin 2017 (https://www.originlab.com/).

3. Results

3.1. Threshold for the constraint of *LUE* by *VPD*

The relationship between *VPD* and *LUE* showed a threshold at all sites (Figure 2). When *VPD* was below the threshold, *LUE* decreased rapidly, with a decreasing ratio of 2.0×10^{-4} to 2.2×10^{-3} gC μmol photon kPa^{-1}, but when *VPD* was above the threshold, the decreasing ratio reduced to between 4.0×10^{-6} and 3.0×10^{-4} gC μmol photon kPa^{-1}. This represents a decrease of 86.4% to 98.0% compared with the value below the threshold; that is, the constraint effect was small when *VPD* exceeds the threshold. Further, a threshold also existed under different *SMC* conditions at one single site (Figure 3) for all four ranges of *SMC*. When *VPD* exceeds the threshold, the slope of the *VPD*-*LUE* relationship decreased by 77.3% to 93.3%.

3.2. Effect of *SMC* on the threshold

We analyzed changes in the *VPD* threshold in response to changes in *SMC* to evaluate the relative impacts of *SMC* on *LUE* (Figure 3). The threshold differed significantly between the different *SMC* regimes, with *VPD* values of 0.9 kPa at *SMC* ranging from 30% to 40%, 1.0 kPa at *SMC* ranging from 20% to 30%, and 1.8 kPa at *SMC* ranging from 10% to 20%, 2.5 kPa at SMC ranging from 0% to 10%. That is, the *VPD* threshold increased with decreasing *SMC*.

Moreover, the reduction of *LUE* caused by *VPD* alone (f*LUE*) also changed with *SMC* (Figure 4). f*LUE* increased with increasing *SMC*, with f*LUE* of 49.4% to 50.1% in the moister region (Daman and Sidaoqiao) and only 17.3% to 19.1% in the more arid region (Hunhe and Huyang). In contrast, r*LUE* increased with decreasing *SMC*, with the largest values in the two drier regions.

3.3 Interactions among *VPD*, *SMC*, and *LUE*

We calculated Pearson's *r* between *SMC* and *LUE*, and analyzed how *r* changed with increasing *VPD* to clarify the interactions among *VPD*, *SMC*, and *LUE* (Figure 5). The

correlation weakened with increasing *VPD* until it reached a threshold, then increased thereafter. When *VPD* was below the threshold, the absolute value of *r* decreased, sometimes to 0, with increasing *VPD*. Therefore, the effect of *SMC* on *LUE* decreased with increasing *VPD* when *VPD* was below the threshold. However, when *VPD* exceeds a threshold, the absolute value of *r* increased with increasing *VPD*, indicating that the importance of *SMC* increased with decreasing *VPD*.

The soil heat fluxes and soil temperature also showed pronounced changes in response to *VPD* (Figure 6). With increasing *VPD*, all soil heat fluxes and soil temperature increased abruptly, indicating the existence of a threshold, whereas *AET* decreased with increasing *VPD* (Figure S1).

4. Discussion

Previous studies have emphasized the constraint of *LUE* by either *VPD* (Yuan et al., 2019) or *SMC* (Stocker et al., 2018), but our results demonstrate that both factors play essential roles in how water stress limits *LUE*, and that their relative importance differs at different levels of water stress.

4.1. Role of *VPD* in constraining *LUE*

The rate of *VPD* induced *LUE* reduction decreased greatly, by 86.4% to 98.0%, when *VPD* crossed a threshold, which existed both for multiple sites with different water moisture regimes and for one site with different water conditions (Figure 4). Moreover, soil heat fluxes and temperature increased abruptly with rising *VPD*, whereas *AET* decreased simultaneously (Figure S1). According to an empirical model of the relationship between *VPD* and *LUE* (Oren et al., 1999), the rate of stomatal decrease would slow when *VPD* increased beyond a large value (Novick et al., 2016). Hence, the rate of *LUE* decrease would decrease significantly above

a threshold (Fletcher et al., 2007). With the reduction of stomatal conductance, *AET* and the cooling effect from this water loss would decrease. As a result, soil temperature increased when *VPD* increases above a threshold (Forzieri et al., 2020). The abrupt change of soil heat flux and *AET* further supported the existence of a threshold, indicating that the exchanges of water and heat between soil, plant and atmosphere also changed near the threshold. The strength of the correlation (|*r*|) between *SMC* and *LUE* decreased greatly with rising *VPD* when *VPD* was below the threshold but increased with rising *VPD* when *VPD* exceeded the threshold (Figure 5). The variation of Pearson's *r* indicates that *SMC* constraint on *LUE* decreased with rising *VPD* below the threshold, which resulted from initial control of *VPD* on *AET* and *LUE*. However, *SMC* constraint on *LUE* increased with rising *VPD* when *VPD* was above the threshold because of vegetation water stress and the decrease of *VPD* constraint on *LUE*. Therefore, the variation of Pearson's r could also support the dynamic *VPD* constraint on *LUE*.

Our results indicate different linear relationships between *VPD* and *LUE* blow and above the threshold. The rate of change in *LUE* above the threshold was less than 25% of the rate below the threshold, and as low as 2% of that rate. The strength of the correlation (|*r*|) between *SMC* and *LUE* decreased greatly with rising *VPD* below the threshold. Therefore, *VPD* had the strongest effect on *LUE* when *VPD* was below the threshold. The effect of *VPD* on stomatal conductance and *LUE* was greater when *VPD* was below the threshold, which agrees with an empirical formula developed for stomatal conductance (Oren et al., 1999). On the other hand, the constraint of *LUE* by *VPD* would be overestimated if all high *VPD* levels were used to represent water limitation, as there is no continuous significant decrease of *LUE* when *VPD* exceeds a threshold. The overestimation of *VPD* constraint was also present in a previous yield loss simulation, in which the crop yield reduction caused by *VPD* constraint of *LUE* was overestimated by a factor of two, mainly as a result of the failure to capture the slower decrease of *LUE* when *VPD* is above a threshold (Rigden et al., 2020). *VPD* limits photosynthesis by

decreasing stomatal conductance, but this limitation will not significantly reduce photosynthesis after a high *VPD* is reached (Grossiord et al., 2020). Thus, reduction of *LUE* caused by *VPD* constraint decreases above the threshold.

4.2. Role of *SMC* in constraint of *LUE*

The reduction of *LUE* decreased greatly with decreasing *SMC*, which also indicates a difference in the constraint of *LUE* by *SMC* and *VPD*. The relationship between *SMC* and *LUE* showed a turning point with rising *VPD*. The absolute value of *r* between *SMC* and *LUE* first decreased with increasing *VPD* and then increased above the threshold. Pearson's *r* between *SMC* and *LUE* could indicate the strength of *SMC* effect on *LUE*. Thus, the relative importance of *SMC* increased and the effect of *SMC* on *LUE* was stronger when *VPD* was above the threshold. Initially, rising *VPD* would significantly decrease *AET* by reducing stomatal conductance when *VPD* was below the threshold (Novick et al., 2016). *AET* and heat exchange therefore changed with increasing *VPD* (Figure 6, Figure S1). Consequently, the consumption of *SMC* initially decreases owing to decreasing *AET* (Anderegg and Venturas, 2020), which would weaken the relationship between *SMC* and *LUE*. However, with *VPD* continuing to increase, available water would decrease, leading to increasing water stress (Grossiord et al., 2020). Therefore, *SMC*, which represents the direct source of water available to the plant, would be essential for maintenance of photosynthesis and other processes as *VPD* continues to increase (Trugman et al., 2018). Under these circumstances, *SMC* becomes vital to maintaining photosynthesis. In the two driest regions (Hunhe and Huyang), the lower threshold for *VPD* (based on $|r|$ in Figure 5) also supports this hypothesis. The lower threshold indicated that *SMC* was more important at Hunhe and Huyang owing to their lower *SMC*, which made photosynthesis more depend on the direct water resource represented by *SMC*.

With *SMC* decreasing, the threshold of *VPD* constraint for *LUE* become larger, further

reduction of *LUE* created by *VPD* decreased, with a reduction of *VPD* contribution to the total constraint to 49.4% to 50.1% in moister region and a reduction of *VPD* constraint to only 17.3% to 19.1% in more arid region (Figure 4). Therefore, *VPD* constraint of *LUE* was more important in moister regions, whereas *SMC* was more important in more arid regions. Hence, the different importance of *VPD* and *SMC* in limiting *LUE* may have resulted from different water regimes. Reduction of *LUE* by *VPD* constraint was larger in more humid regions, thus, *VPD* would play the dominant role in limiting *LUE* in such regions (Novick et al., 2016; Yuan et al., 2019). Furthermore, the reduction of *LUE* by *SMC* constraint was larger in drier regions, *SMC* would play the dominant role in limiting *LUE* in such regions (L. Liu et al., 2020; Stocker et al., 2018). A previous study also suggested that both *VPD* and *SMC* are important in the constraint of *LUE* (Rigden et al., 2020). *SMC* determined the range of the reduction, but the constraint effect of *VPD* was stronger than *SMC* when *VPD* was below the threshold. Consequently, considering only *VPD* or *SMC* would result in considerable errors in simulating photosynthesis (Rigden et al., 2020).

4.3. Implications for carbon cycle simulation

The relative constraints caused by *VPD* and *SMC* varied with decreasing *SMC* (Figure 4), indicating that variation of *SMC* would change the relationships among *VPD*, *SMC*, and *LUE*. These changes would regulate the vegetation responses to water stress, thereby changing photosynthesis and the carbon cycle in arid and semi-arid regions (Rogers et al., 2017; Stocker et al., 2019). The precipitation in arid regions fluctuates greatly, causing high variation of *SMC*. This exacerbates the impacts of water stress because photosynthesis of plants in arid regions can be more sensitive to changes in water availability (Gonsamo et al., 2019). Consequently, the relationships among *VPD*, *SMC*, and *LUE* will change frequently in response to a large variation of *SMC* (Stocker et al., 2019). This will lead to high uncertainty in simulation of the

carbon cycle in arid ecosystems. Specifically, as water conditions change, the threshold and reduction for *VPD* constraint of *LUE* will change, but it is essential to account for these changes to reduce the uncertainty in simulations of the carbon cycle in arid regions (Trugman et al., 2018; Zhang et al., 2018). We analyzed how *LUE* changed with different *VPD* and *SMC* in five sites. However, biotic processes and characters are critical for vegetation photosynthesis. *LUE* would significantly vary with vegetation type, indicating that vegetation type significantly affects *LUE* (Fei et al., 2019). For example, *LUE* in cropland was different from grassland and forest, which resulted from management practices (Allen et al., 2005).

5. Conclusion

Our study revealed that both *VPD* and *SMC* played important roles in how water limitations (i.e., an imbalance between water demand, represented by *VPD*, and supply, represented by *SMC*) constrained *LUE*. We found clear evidence for a threshold for constraint of *LUE* by *VPD*. The rate of *LUE* reduction at *VPD* above the threshold was only 3.6% to 23.1% of that below the threshold. Furthermore, the threshold and the magnitude of the reduction of *LUE* above that threshold were affected by *SMC*. The *VPD* threshold increased with decreasing *SMC*. With decreasing *SMC* at different sites, the reduction of *VPD* constraint decreased, with *VPD* contribution of 49.4% to 50.1% of the total at moister sites, but decreasing to 17.3% to 19.1% in more arid regions. Consequently, *VPD* had a more important effect on *LUE* in moister regions, whereas *SMC* became more important in more arid regions. The interactions among *VPD*, *SMC*, and *LUE* and soil heat flux also support the relative strengths of the constraint of *LUE* created by *VPD* and *SMC*. The strength of the correlation between *SMC* and *LUE* decreased below the threshold, then increased again above it, whereas soil temperature and heat flux increased with increasing *VPD*, which resulted in the changes in the relative roles of *VPD* and *SMC*.

This study was conducted in arid and semi-arid region to analyze the constraint process of

VPD and *SMC,* aiming to quantify the relative role of *VPD* and *SMC* in water limitation on *LUE*. However, the constraint process in moisture region may differ from that in arid and semi-arid region. To illustrate the water limitation process, therefore, mechanistic understanding of constraint of *VPD* and *SMC* are needed in moist region to clarify the interaction process among *VPD*, *SMC*, and *LUE*, which may differ in moist regions and drylands.

Data availability statement

The authors confirm that the data supporting the findings of this study are available from dataset of Heihe Watershed Allied Telemetry Experimental Research (HiWATER) Monitoring & Big Data Center for Three Poles.

Acknowledgements

This work was supported by National Natural Science Foundation of China (41991230), and "the Fundamental Research Funds for the Central Universities". The data in this study are obtained from Heihe Watershed Allied Telemetry Experimental Research (HiWATER) field campaigns, and we appreciate all people contribute to this project. We also thank the editors and reviewers for improving this manuscript on this work. A special thanks to Dongxing Wu for method of interpolation.

References:

Ahmed, M., Else, B., Eklundh, L., Ardö, J., Seaquist, J., 2017. Dynamic response of ndvi to soil moisture variations during different hydrological regimes in the sahel region. International Journal of Remote Sensing 38, 5408–5429. https://doi.org/10.1080/01431161.2017.1339920

Allen, C.B., Will, R.E., McGarvey, R.C., Coyle, D.R., Coleman, M.D., 2005. Radiation-use efficiency and gas exchange responses to water and nutrient availability in irrigated and fertilized stands of sweetgum and sycamore. Tree Physiology 25, 191–200. https://doi.org/10.1093/treephys/25.2.191

Anderegg, W.R.L., Venturas, M.D., 2020. Plant hydraulics play a critical role in Earth system fluxes. New Phytologist 226, 1535–1538. https://doi.org/10.1111/nph.16548

Bartletta, M.K., Klein, T., Jansen, S., Choat, B., Sack, L., 2016. The correlations and sequence of plant stomatal, hydraulic, and wilting responses to drought. Proceedings of the National Academy of Sciences of the United States of America 113, 13098–13103. https://doi.org/10.1073/pnas.1604088113

Biederman, J.A., Scott, R.L., Bell, T.W., Bowling, D.R., Dore, S., Garatuza-Payan, J., Kolb, T.E., Krishnan, P., Krofcheck, D.J., Litvak, M.E., Maurer, G.E., Meyers, T.P., Oechel, W.C., Papuga, S.A., Ponce-Campos, G.E., Rodriguez, J.C., Smith, W.K., Vargas, R., Watts, C.J., Yepez, E.A., Goulden, M.L., 2017. CO2 exchange and evapotranspiration across dryland ecosystems of southwestern North America. Global Change Biology 23, 4204–4221. https://doi.org/10.1111/gcb.13686

Cleverly, J., Vote, C., Isaac, P., Ewenz, C., Harahap, M., Beringer, J., Campbell, D.I., Daly, E., Eamus, D., He, L., Hunt, J., Grace, P., Hutley, L.B., Laubach, J., McCaskill, M., Rowlings, D., Rutledge Jonker, S., Schipper, L.A., Schroder, I., Teodosio, B., Yu, Q., Ward, P.R., Walker, J.P., Webb, J.A., Grover, S.P.P., 2020. Carbon, water and energy fluxes in agricultural systems of Australia and New Zealand. Agricultural and Forest Meteorology 287, 107934. https://doi.org/10.1016/j.agrformet.2020.107934

Falge, E., Baldocchi, D., Olson, R., Anthoni, P., Aubinet, M., Bernhofer, C., Burba, G., Ceulemans, R., Clement, R., Dolman, H., Granier, A., Gross, P., Grünwald, T., Hollinger, D., Jensen, N.O., Katul, G., Keronen, P., Kowalski, A., Lai, C.T., Law, B.E., Meyers, T., Moncrieff, J., Moors, E., Munger, J.W., Pilegaard, K., Rannik, Ü., Rebmann, C., Suyker, A., Tenhunen, J., Tu, K., Verma, S., Vesala, T., Wilson, K., Wofsy, S., 2001. Gap filling strategies for defensible annual sums of net ecosystem exchange. Agricultural and Forest Meteorology 107, 43–69. https://doi.org/10.1016/S0168-1923(00)00225-2

Fei, X.H., Song, Q.H., Zhang, Y.P., Yu, G.R., Zhang, L.M., Sha, L.Q., Liu, Y.T., Xu, K., Chen, H., Wu, C.S., Chen, A.G., Zhang, S. Bin, Liu, W.W., Huang, H., Deng, Y., Qin, H.L., Li, P.G., Grace, J., 2019. Patterns and Controls of Light Use Efficiency in Four Contrasting Forest Ecosystems in

Yunnan, Southwest China. Journal of Geophysical Research: Biogeosciences 124, 293–311. https://doi.org/10.1029/2018JG004487

Fletcher, A.L., Sinclair, T.R., Allen, L.H., 2007. Transpiration responses to vapor pressure deficit in well watered “slow-wilting” and commercial soybean. Environmental and Experimental Botany 61, 145–151. https://doi.org/10.1016/j.envexpbot.2007.05.004

Forzieri, G., Miralles, D.G., Ciais, P., Alkama, R., Ryu, Y., Duveiller, G., Zhang, K., Robertson, E., Kautz, M., Martens, B., Jiang, C., Arneth, A., Georgievski, G., Li, W., Ceccherini, G., Anthoni, P., Lawrence, P., Wiltshire, A., Pongratz, J., Piao, S., Sitch, S., Goll, D.S., Arora, V.K., Lienert, S., Lombardozzi, D., Kato, E., Nabel, J.E.M.S., Tian, H., Friedlingstein, P., Cescatti, A., 2020. Increased control of vegetation on global terrestrial energy fluxes. Nature Climate Change 10, 356–362. https://doi.org/10.1038/s41558-020-0717-0

Gonsamo, A., Chen, J.M., He, L., Sun, Y., Rogers, C., Liu, J., 2019. Exploring SMAP and OCO-2 observations to monitor soil moisture control on photosynthetic activity of global drylands and croplands. Remote Sensing of Environment 232, 111314. https://doi.org/10.1016/j.rse.2019.111314

Grossiord, C., Buckley, T.N., Cernusak, L.A., Novick, K.A., Poulter, B., Siegwolf, R.T.W., Sperry, J.S., McDowell, N.G., 2020. Plant responses to rising vapor pressure deficit. New Phytologist 226, 1550–1566. https://doi.org/10.1111/nph.16485

Hsiao, J., Swann, A.L.S., Kim, S.-H., 2019. Maize yield under a changing climate: The hidden role of vapor pressure deficit. Agricultural and Forest Meteorology 279, 107692. https://doi.org/10.1016/j.agrformet.2019.107692

Isaac, P., Cleverly, J., McHugh, I., Van Gorsel, E., Ewenz, C., Beringer, J., 2017. OzFlux data: Network integration from collection to curation. Biogeosciences 14, 2903–2928. https://doi.org/10.5194/bg-14-2903-2017

Lanning, M., Wang, L., Scanlon, T.M., Vadeboncoeur, M.A., Adams, M.B., Epstein, H.E., Druckenbrod, D., 2019. Intensified vegetation water use under acid deposition. Science Advances 5, 1–10. https://doi.org/10.1126/sciadv.aav5168

Li, X., Cheng, G., Liu, S., Xiao, Q., Ma, M., Jin, R., Che, T., Liu, Q., Wang, W., Qi, Y., Wen, J., Li, H.,

Zhu, G., Guo, J., Ran, Y., Wang, S., Zhu, Z., Zhou, J., Hu, X., Xu, Z., 2013. Heihe watershed allied telemetry experimental research (HiWater) scientific objectives and experimental design. Bulletin of the American Meteorological Society 94, 1145–1160. https://doi.org/10.1175/BAMS-D-12-00154.1

Liu, L., Gudmundsson, L., Hauser, M., Qin, D., Li, S., Seneviratne, S.I., 2020. Soil moisture dominates dryness stress on ecosystem production globally. Nature Communications 11, 4892. https://doi.org/10.1038/s41467-020-18631-1

Liu, S.M., Xu, Z.W., Wang, W.Z., Jia, Z.Z., Zhu, M.J., Bai, J., Wang, J.M., 2011. A comparison of eddy-covariance and large aperture scintillometer measurements with respect to the energy balance closure problem. Hydrology and Earth System Sciences 15, 1291–1306. https://doi.org/10.5194/hess-15-1291-2011

Liu, Y., Kumar, M., Katul, G.G., Feng, X., Konings, A.G., 2020. Plant hydraulics accentuates the effect of atmospheric moisture stress on transpiration. Nature Climate Change 10, 691–695. https://doi.org/10.1038/s41558-020-0781-5

Mccarter, C.P.R., Price, J.S., 2014. Ecohydrology of Sphagnum moss hummocks: Mechanisms of capitula water supply and simulated effects of evaporation. Ecohydrology 7, 33–44. https://doi.org/10.1002/eco.1313

McDowell, N.G., Allen, C.D., 2015. Darcy's law predicts widespread forest mortality under climate warming. Nature Climate Change 5, 669–672. https://doi.org/10.1038/nclimate2641

Monteith.J.L., C., J., Moss, 1977. Climate and the Efficiency of Crop Production in Britain [and Discussion]. Philosophical Transactions of the Royal Society B: Biological Sciences 281, 277–294.

Novick, K.A., Ficklin, D.L., Stoy, P.C., Williams, C.A., Bohrer, G., Oishi, A.C., Papuga, S.A., Blanken, P.D., Noormets, A., Sulman, B.N., Scott, R.L., Wang, L., Phillips, R.P., 2016. The increasing importance of atmospheric demand for ecosystem water and carbon fluxes. Nature Climate Change 6, 1023–1027. https://doi.org/10.1038/nclimate3114

Oren, R., Sperry, J.S., Katul, G.G., Pataki, D.E., Ewers, B.E., Phillips, N., Schäfer, K.V.R., 1999. Survey and synthesis of intra- and interspecific variation in stomatal sensitivity to vapour pressure deficit.

Plant, Cell and Environment 22, 1515–1526. https://doi.org/10.1046/j.1365-3040.1999.00513.x

provided by EUROFLUX, D., Rebmann, C., Schulze, E., Tenhunen, J., Gr\\"unwald, T., Bernhofer, C., Moors, E., Elbers, J.A., Dolman, H., Pilegaard, K., others, 2001. Gap filling strategies for long term energy flux data sets. Agricultural and Forest Meteorology 107, 71–77.

Rigden, A.J., Mueller, N.D., Holbrook, N.M., Pillai, N., Huybers, P., 2020. Combined influence of soil moisture and atmospheric evaporative demand is important for accurately predicting US maize yields. Nature Food 1, 127–133. https://doi.org/10.1038/s43016-020-0028-7

Rogers, A., Medlyn, B.E., Dukes, J.S., Bonan, G., von Caemmerer, S., Dietze, M.C., Kattge, J., Leakey, A.D.B., Mercado, L.M., Niinemets, Ü., Prentice, I.C., Serbin, S.P., Sitch, S., Way, D.A., Zaehle, S., 2017. A roadmap for improving the representation of photosynthesis in Earth system models. New Phytologist 213, 22–42. https://doi.org/10.1111/nph.14283

Seneviratne, S.I., Corti, T., Davin, E.L., Hirschi, M., Jaeger, E.B., Lehner, I., Orlowsky, B., Teuling, A.J., 2010. Investigating soil moisture-climate interactions in a changing climate: A review. Earth-Science Reviews 99, 125–161. https://doi.org/10.1016/j.earscirev.2010.02.004

Stocker, B.D., Zscheischler, J., Keenan, T.F., Prentice, I.C., Peñuelas, J., Seneviratne, S.I., 2018. Quantifying soil moisture impacts on light use efficiency across biomes. New Phytologist 218, 1430–1449. https://doi.org/10.1111/nph.15123

Stocker, B.D., Zscheischler, J., Keenan, T.F., Prentice, I.C., Seneviratne, S.I., Peñuelas, J., 2019. Drought impacts on terrestrial primary production underestimated by satellite monitoring. Nature Geoscience 12, 264–270. https://doi.org/10.1038/s41561-019-0318-6

Stocker, T.F., Qin, D., Plattner, G.K., Alexander, L. V, Allen, S.K., Bindoff, N.L., Bréon, F.M., Church, J.A., Cubasch, U., Emori, S., 2013. IPCC, 2013: Technical Summary. In: Climate Change 2013: The Physical Science Basis. Contribution of Working Group I to the Fifth Assessment Report of the Intergovernmental Panel on Climate Change [Stocker, T.F., D. Qin, G.-K. Plattner, M. Tignor, S.K. All.

Taylor, N., Price, J., Strack, M., 2016. Hydrological controls on productivity of regenerating Sphagnum in a cutover peatland. Ecohydrology 9, 1017–1027. https://doi.org/10.1002/eco.1699

Trugman, A.T., Medvigy, D., Mankin, J.S., Anderegg, W.R.L., 2018. Soil Moisture Stress as a Major

Driver of Carbon Cycle Uncertainty. Geophysical Research Letters 45, 6495–6503. https://doi.org/10.1029/2018GL078131

Venturini, V., Rodriguez, L., Bisht, G., 2011. A comparison among different modified priestley and taylor equations to calculate actual evapotranspiration with MODIS data. International Journal of Remote Sensing 32, 1319–1338. https://doi.org/10.1080/01431160903547965

Wang, H., Li, X., Ma, M., Geng, L., 2019. Improving estimation of gross primary production in dryland ecosystems by a model-data fusion approach. Remote Sensing 11. https://doi.org/10.3390/rs11030225

Wang, M., Wu, J., Lafleur, P.M., Luan, J., Chen, H., Zhu, X., 2018. Temporal shifts in controls over methane emissions from a boreal bog. Agricultural and Forest Meteorology 262, 120–134. https://doi.org/10.1016/j.agrformet.2018.07.002

Wu, J., Jing, Y., Guan, D., Yang, H., Niu, L., Wang, A., Yuan, F., Jin, C., 2013. Controls of evapotranspiration during the short dry season in a temperate mixed forest in Northeast China. Ecohydrology 6, 775–782. https://doi.org/10.1002/eco.1299

Yu, G.R., Wen, X.F., Sun, X.M., Tanner, B.D., Lee, X., Chen, J.Y., 2006. Overview of ChinaFLUX and evaluation of its eddy covariance measurement. Agricultural and Forest Meteorology 137, 125–137. https://doi.org/10.1016/j.agrformet.2006.02.011

Yuan, W., Cai, W., Xia, J., Chen, J., Liu, S., Dong, W., Merbold, L., Law, B., Arain, A., Beringer, J., Bernhofer, C., Black, A., Blanken, P.D., Cescatti, A., Chen, Y., Francois, L., Gianelle, D., Janssens, I.A., Jung, M., Kato, T., Kiely, G., Liu, D., Marcolla, B., Montagnani, L., Raschi, A., Roupsard, O., Varlagin, A., Wohlfahrt, G., 2014. Global comparison of light use efficiency models for simulating terrestrial vegetation gross primary production based on the LaThuile database. Agricultural and Forest Meteorology 192–193, 108–120. https://doi.org/10.1016/j.agrformet.2014.03.007

Yuan, W., Zheng, Y., Piao, S., Ciais, P., Lombardozzi, D., Wang, Y., Ryu, Y., Chen, G., Dong, W., Hu, Z., Jain, A.K., Jiang, C., Kato, E., Li, S., Lienert, S., Liu, S., Nabel, J.E.M.S., Qin, Z., Quine, T., Sitch, S., Smith, W.K., Wang, F., Wu, C., Xiao, Z., Yang, S., 2019. Increased atmospheric vapor pressure deficit reduces global vegetation growth. Science Advances 5, 1–13.

https://doi.org/10.1126/sciadv.aax1396

Zhang, X., Dong, K., Xu, K., Zhang, K., Jin, X., Yang, M., Zhang, Y., Wang, X., Han, C., Yu, J., Li, D., 2018. Barley stripe mosaic virus infection requires PKA-mediated phosphorylation of γb for suppression of both RNA silencing and the host cell death response. New Phytologist 218, 1570–1585. https://doi.org/10.1111/nph.15065

Table 1. Locations and climate data of the study sites used in this study.

Site	Longitude (°N)	Latitude (°E)	*MAT* (°C)	*MAP* (mm)
Arou	38.0473	100.4643	−0.29	444.7
Daman	38.85551	100.3722	6.93	135.7
Sidaoqiao	42.0012	101.1374	10.06	37.13
Hunhe	41.9903	101.1335	10.04	35.53
Huyang	41.9928	101.1236	10.33	26.00

MAT, mean annual temperature; *MAP*, mean annual precipitation.

Appendix: Figure S1 and Table S1

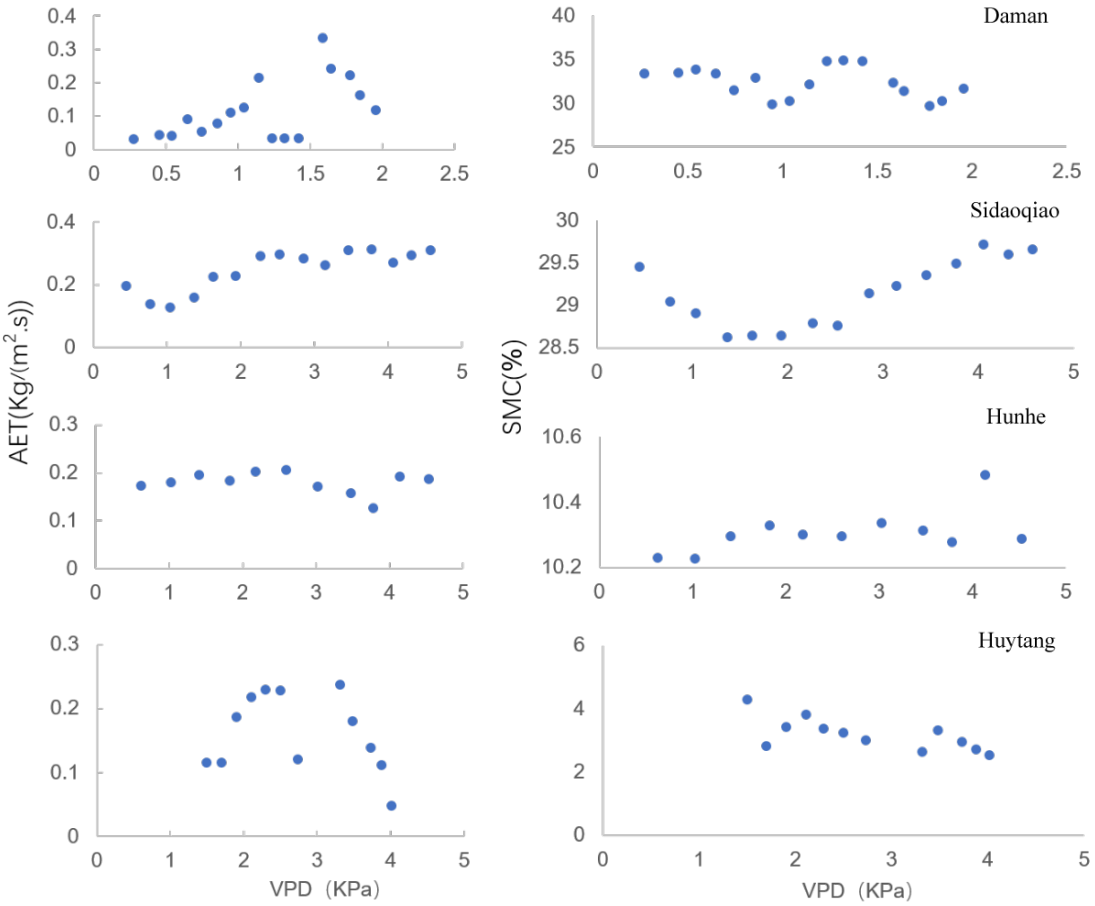

Figure S1. Response of actual evapotranspiration (*AET*) and soil moisture content (*SMC*) to rising vapor-pressure deficit (*VPD*).

Table S1. Predicted vs. observed net ecosystem exchange (*NEE*) at the five study sites.

	Arou	Daman	Sidaoqiao	Hunhe	Huyang
R^2	0.6230	0.7625	0.6242	0.5878	0.7624
n	515	368	1149	1006	1093